Computers and Geotechnics 36 (2009) 1200–1206

Contents lists available at ScienceDirect

Computers and Geotechnics

journal homepage: www.elsevier.com/locate/compgeo

Upscaling of Navier–Stokes equations in porous media: Theoretical, numerical and experimental approach

Guillermo A. Narsilio [a,*], Olivier Buzzi [b], Stephen Fityus [b], Tae Sup Yun [c], David W. Smith [d]

[a] Melbourne Engineering Research Institute (MERIT), Department of Civil and Environmental Engineering, The University of Melbourne, Parkville, VIC 3010, Australia
[b] Centre for Geotechnical and Materials Modelling, The School of Engineering, The University of Newcastle, Callaghan, NSW 2308, Australia
[c] Department of Civil and Environmental Engineering, Lehigh University, 13 East Packer Avenue, Bethlehem, PA 18015, USA
[d] Faculty of Engineering, Computing and Mathematics, The University of Western Australia (M017), Crawley, WA 6009, Australia

ARTICLE INFO

Article history:
Received 9 October 2008
Received in revised form 19 March 2009
Accepted 11 May 2009
Available online 13 June 2009

Keywords:
Fluid flow
Porous media
Navier–Stokes
Darcy's law
micro-CT
Hydraulic conductivity

ABSTRACT

The accurate estimation of hydraulic conductivity is important for many geotechnical engineering applications, as the presence of fluids affects all aspects of soil behaviour, including its strength. Darcy's law is the key experimental (or phenomenological) equation employed to model ground water flow. Yet, this phenomenological equation can be linked to a more fundamental microscale model of flow through the pore spaces of the porous material. This paper provides an experimental verification of the relationships between Darcy's law (macroscale) and the Navier–Stokes equations (microscale) for actual complex pore geometries of a granular material. The pore geometries are experimentally obtained through state-of-the-art X-ray computer assisted micro-tomography. From the numerical modelling of the microscale flow based on actual pore geometries, it is possible to quantify and visualize the development of pore-scale fluid preferential flow-paths through the porous material, and to assess the importance of pore connectivity in soil transport properties.

1. Introduction

Accurate estimates of soil properties are important for a range of engineering applications, including geotechnical, geoenvironmental and resources engineering. The estimation of hydraulic conductivity in particular, plays a central role in many disciplines including hydrology, geoenvironmental engineering and hydrocarbon recovery. The presence of fluids affects all aspects of soil behaviour, including the soil's chemical, mechanical, and geo-biological processes [1,2].

The understanding of fluid flow through porous media began in the eighteenth century. Daniel Bernoulli first recognised the importance of energy conservation in the analysis of fluid flow. Following the work by Pierre Laplace, Claude-Louis Navier presented the differential equations to describe pressure and velocity in unsteady three-dimensional viscous flow, which later become known as the Navier–Stokes equations. Both Jean Louis Poiseuille and Gotthilf Hagen studied low-velocity flow in capillary tubes and arrived at similar semi-empirical equations of surprising accuracy (the so-called Hagen–Poiseuille equation), which was later shown to corroborate the analytical solution based on Newton's viscosity law published by Wiedman in 1859 and by Neumann and Hagenbach in 1860 [3,4]. These formulations form the theoretical basis for Darcy's experimental findings [5]. In 1856, Henry Darcy realized that the rate of seepage Q (volume/time) through a porous medium of cross-sectional area A, can be considered to be proportional to the hydraulic gradient i; or symbolically, $v = Q/A = k \cdot i$, where v is the effective flow velocity and k is the hydraulic conductivity. Darcy's law applies in the laminar regime, which occurs for small Reynolds numbers R_e (R_e is the ratio of inertial to viscous forces; $R_e = v \cdot d_e/\mu$, where v is the velocity of the fluid, d_e is the effective pore diameter of the soil skeleton and μ is the kinematic viscosity of water [6,7]).

Darcy's law is the key *phenomenological* equation used to estimate ground water flow. Yet this phenomenological formulation can be linked to more fundamental microscale governing equations based on Stokes' law (see for example chapters IV and V in Bear, 1988). This paper provides an experimental verification of the relationships between Darcy's law (at the macroscale) and the Navier–Stokes equations (at the microscale) applied to actual complex pore geometries of a granular material. Here the hydraulic conductivity is first estimated using a modified hydraulic conductivity apparatus (according to Australian Standard AS 1289.6.7.1-2001). It is then again estimated independently using a finite element analysis of the same material, with actual pore geometries that are obtained experimentally through state-of-the-art X-ray computer assisted micro-tomography. No fitting

* Corresponding author. Tel.: +61 3 8344 4659; fax: +61 3 8344 6215.
E-mail addresses: narsilio@unimelb.edu.au (G.A. Narsilio), Olivier.Buzzi@newcastle.edu.au (O. Buzzi), Stephen.Fityus@newcastle.edu.au (S. Fityus), taesup@lehigh.edu (T.S. Yun), davidw.smith@uwa.edu.au (D.W. Smith).

0266-352X/$ - see front matter © 2009 Elsevier Ltd. All rights reserved.
doi:10.1016/j.compgeo.2009.05.006

Nomenclature

A	cross-sectional area	Q	rate of seepage
A_{pore}	net conductive cross-section area (pores only)	R_e	Reynolds number
C	pore conductance	R_s	force resisting the motion of the fluid inside the pore
d_{50}	mean particle size diameter	$\mathbf{R}$	resisting force vector
$\mathbf{F}$	volume force vector	v	effective fluid velocity
g	acceleration due to gravity	$\mathbf{v}$	effective fluid velocity vector (with v_x, v_y and v_z components)
h	total head		
i	hydraulic gradient	z	elevation head
k	hydraulic conductivity	γ_w	unit weight of fluid (e.g., water)
K	intrinsic permeability, $K = k \cdot \eta/(\rho_w \cdot g)$	η	dynamic fluid viscosity
L	specimen length (in the direction of fluid flow)	μ	kinematic fluid viscosity
n	porosity	ρ_w	fluid density (e.g., water)
p	pressure	σ	local coordinate of a streamline

procedure was followed. We investigate the compatibility of Navier–Stokes equations at microscale and Darcy's law at macroscale. The key question asked here is whether both approaches lead to the same result, and so set the basis for development of technologies where a microscale analysis coupled with modern imaging techniques may be used as alternative for traditional methods for estimating soil parameters [8].

2. Materials and experimental procedures

To minimize the number of variables involved in our analyses, we use a very uniform granular material with well rounded particles (in this case glass beads) of mean size $d_{50} \approx 0.5$ mm. A medium density packing of these grains is subsequently subjected to: (1) constant head permeability tests to determine its hydraulic conductivity, and (2) X-ray micro-computerized tomography (micro-CT) to obtain the 3D pore (and solid) geometries of the same assemblage of grains. Details of these follow.

2.1. Hydraulic conductivity tests

To achieve the (maximum) desired spatial resolution of the pore geometries, i.e. 5 μm restrictions on specimen sizes are imposed by the micro-CT (details are provided in the next section). For this reason, classical permeability apparatus could not be used, and a special permeability cell was designed to accommodate these smaller-than-standard specimens without compromising accuracy of the results (see Fig. 1).

The permeability cell is made of PVC with a wall thickness of 5 mm. The specimen (inner diameter 10 mm, height 20 mm) is prepared directly in the cell, where the rounded particles are confined between two stainless steel grid-mesh discs and two plastic plugs. Note that even though the specimen dimensions are smaller than that recommended in the standard, the ratio of the maximum grain size to the specimen diameter (1:20) is satisfactory and that the specimen made up of glass beads can be considered as a homogeneous porous medium. As recommended in the standard AS 1289.6.7.1-2001, the permeability cell is connected to a water reservoir at constant head (not represented on the figure) so that water inflow is through the base of the cell and water outflow is through the top part of the cell. The flow is back-calculated from the measured mass of water (scale at ±0.01 g) collected during a given time measured with a stopwatch.

The cell was designed so that it could be placed in the micro-CT scanner without having to unmount the specimen. In particular, its relatively small wall thickness allows scanning without loss of accuracy. This approach ensures that the microstructure scanned is exactly the same as that tested.

Constant head permeability tests are performed with injection pressures ranging from 0.25 kPa to 0.75 kPa. After the permeability tests, the specimen is air dried before being scanned.

2.2. 3D pore geometry estimations

The pore structure of granular materials controls its transport properties [9,10]. Knowing the fabric or geometry of the grain structure (or more precisely, pore space geometry) and fluid properties, allows the estimation of transport parameters [8,9,11]. These microstructures can be accurately estimated using a variety of methods including: (1) obtaining a series of two dimensional thin sections [12,13]; (2) CT, micro-CT and nano-CT [14–16]; and (3) magnetic resonance imaging (MRI). The latter can also be also used to obtain information on pathflow patterns, water content [17] and liquid flow velocity at the pore-scale [18]; however these require more complex experimental setups.

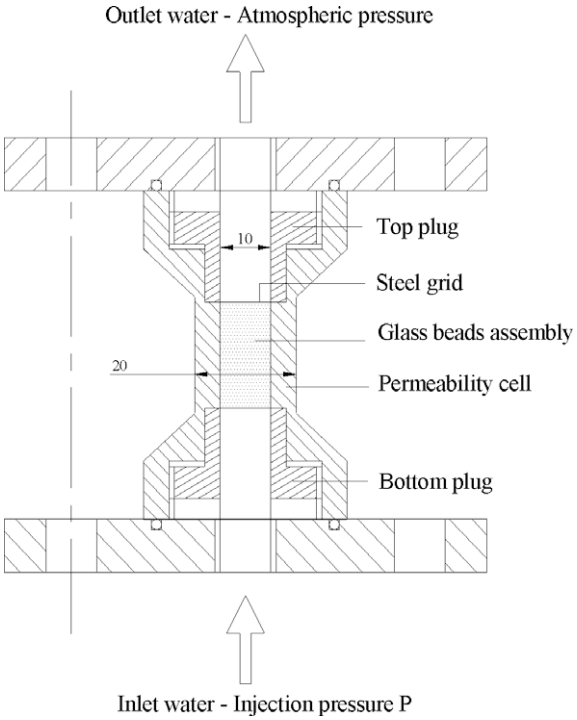

Fig. 1. Experimental setup to measure hydraulic conductivity: detail of the specially designed permeameter cell (dimensions in mm).

We have employed the micro-CT technique to determine the 3D pore geometry of our specimen, which is most accurate for dense materials like glass (silica) that absorb X-rays. A Skyscan 1172 was used to scan the same specimen previously tested using the modified constant head test apparatus, without removing it from the permeameter cell. In this way, exactly the same pore geometry subjected to direct measurement of hydraulic conductivity, is geometrically characterised using the micro-CT scanner.

The tomographic method involves the specimen being positioned between an X-ray source and an X-ray detector, and the specimen being systematically rotated so that a number of 2D radiographs are recorded at different rotation angles between 0° and 360° [19]. The spatial resolution of the images depends on (1) the magnification, given by the ratio of the distance between X-ray source and receiver and the distance between the source and the specimen, (2) the size of the X-ray beam, (3) the pixel size of the detector, and (4) degree of X-ray scattering [19]. In order to achieve a 5 μm resolution (using the micro-CT scanner employed in this work), a sample 10 mm in diameter and 20 mm in height was required.

From hundreds of closely-spaced, parallel 2D radiographs, the internal volume of the specimen is reconstructed using inverse problems techniques, i.e. by tomography [9,19,20]. In this work, we distinguish two phases within the specimen: the solid phase (i.e., the grains) and the fluid phase (i.e., the pore space filled with air). These phases are distinguished by their different X-ray absorption, which leads to different (gray-scale) intensity values. Fig. 2 shows cross-sectional tomographic images that have been reconstructed from the 2D radiographs.

Further image processing allows the rendering of 3D geometries of the pore (and/or grain) network as follows: the 2D slices (like the ones shown in Fig. 2) are additionally enhanced with 'noise' reduction, smoothing and contrast increase [20]. This facilitates the 'segmentation' of the images, where 'gray-scale images' are converted into 'binary images' based on global thresholds for their intensity values. Specialized software is used to convert the 2D (segmented) binary images into 3D volumes. Fig. 3 shows a typical rendering of the glass bead assembly to achieve faithful 3D representations of the microstructure.

3. Multi-scale water flow modelling

Fluid flow in soils can be described at the macroscale using Darcy's law. At the microscale (or, more precisely for the context here, at the pore-scale) the Navier–Stokes equations govern the movement of water within the connected pore spaces. These two approaches (macroscale experimental results and the microscale analysis based on actual pore geometries) are in fact linked. The objective of this study is to compute a hydraulic conductivity from the microscale Navier–Stokes equations based on the geometry

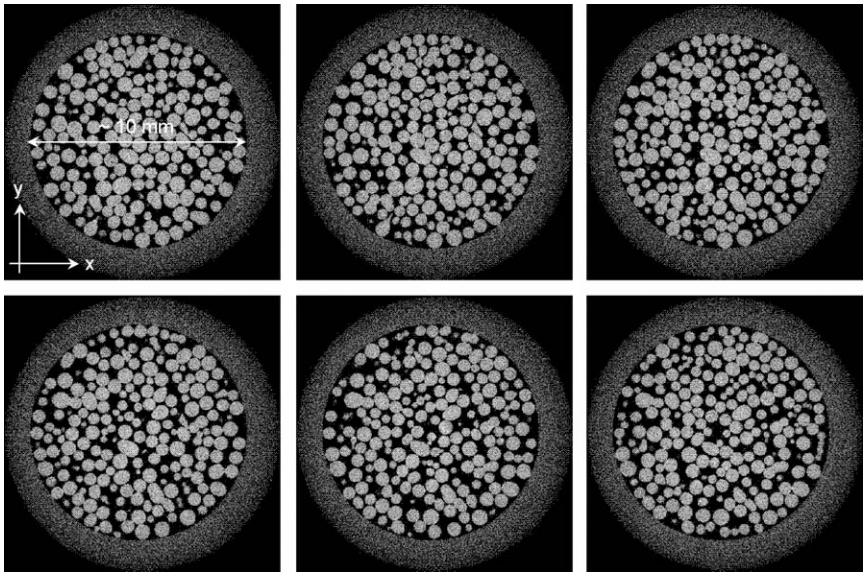

Fig. 2. Sequence of specimen cross-sections reconstructed from 2D radiographs through inversion algorithms. Whiter pixels denote denser material.

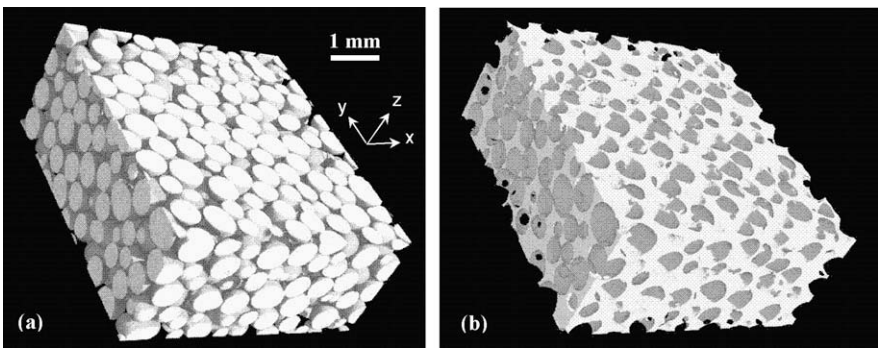

Fig. 3. 3D image of the particle-scale structure of randomly distributed glass beads ($d_{50} \approx 500$ μm): (a) solid particle domain, (b) pore-network domain. (Image rendering by Dr. Alan Jones, Electron Microscopy Unit – U. of Sydney).

found using micro-CT of the sample, and to compare this with the macroscale hydraulic conductivity obtained from traditional permeability tests on relatively large specimens. This section briefly summarizes the theoretical links between macroscale and microscale analyses. Details about the numerical model that simulates Navier–Stokes flow in the pore-network are also provided.

3.1. Governing equations

Darcy's Law: in 1856 Darcy found that the rate of flow Q (volume/unit time) is (i) proportional to the cross-sectional area A of the soil under consideration; (ii) proportional to the difference in total head $\Delta h = (h_1 - h_2)$ over the length L over which fluid flow takes place, and (iii) inversely proportional to that length L. The ratio $\Delta h/L$ is known as hydraulic gradient i. Thus Darcy's law states:

$$v = \frac{Q}{A} = -k\left(\frac{h_1 - h_2}{L}\right) = -k \cdot i \tag{1}$$

where the ratio Q/A is the 'effective' or Darcy velocity v. This phenomenological or experimentally derived law can be generalized for an isotropic 3D porous medium as $\mathbf{v} = -k \cdot \nabla h$, where $\mathbf{v}$ is the effective velocity vector with components v_x, v_y and v_z corresponding to the Cartesian x, y and z coordinates, and ∇h is the hydraulic gradient with components $i_x = \partial h/\partial x$, $i_y = \partial h/\partial y$ and $i_z = \partial h/\partial z$. The 'total head' h arises from the pressure potential p/γ_w, the elevation potential z, and the kinetic energy $v^2/(2g)$, where z is the elevation head with respect to some fixed reference datum, p is pressure, γ_w is the unit weight of the fluid (usually water) and g is the acceleration due to gravity. However for a porous medium, the fluid velocity is usually low and changes in the piezometric head are much larger than the fraction of kinetic energy; so the later contribution is usually neglected, leading to $h \approx p/\gamma_w + z$. This leads Eq. (1) to be reformulated in terms of elevation z and fluid pressure p:

$$\begin{aligned}\mathbf{v} &= -k\left(\frac{\nabla p}{\gamma_w} + \nabla z\right) = -\frac{k}{\rho_w g}(\nabla p + \rho_w g \nabla z) \\ &= -\frac{K}{\eta}(\nabla p + \rho_w g \nabla z)\end{aligned} \tag{2}$$

where ρ_w is the fluid density, η is the fluid dynamics viscosity and K is the intrinsic permeability of the granular medium linked to the hydraulic conductivity k as $K = k \cdot \eta/(\rho_w \cdot g)$.

Incompressible Navier–Stokes equation: The empirical Darcy's formulations (i.e., Eqs. (1) and (2)), can be also derived in a more fundamental way from the physical equations at the microscale using the theory of hydrodynamics [6]. For example, Darcy's law can found by averaging the incompressible Navier–Stokes equations that describe the flow of Newtonian fluids of nearly constant density. We follow the derivation introduced by Bear and Bachmat in the late sixties [6,21]. Assuming that all of the stresses in the flow field are carried out by the porous medium and that the fluid in the pore-network is at constant temperature and density, then the Navier–Stokes equation for fluid flow in the s-direction at a point inside a pore is:

$$\rho_w \frac{\partial v_s}{\partial t} + \rho_w(\mathbf{v} \cdot \nabla)v_s + \frac{\partial p}{\partial s} - R_s = -\rho_w g \frac{\partial z}{\partial s} \tag{3}$$

where ρ_w is the fluid density (commonly water), v_s is the fluid velocity in the s-direction, $\mathbf{v}$ is the fluid velocity field, p is pressure, R_s represents the force resisting the motion of the fluid inside the pore, and the right hand side of Eq. (3) is the body force due to gravity, involving the acceleration due to gravity g and the vertical coordinate z. The resisting force R_s arises from (boundary) drag force of the fluid particles acting on the stationary grains, and is *assumed* to be proportional to the mass–average velocity. This force acts in direction opposite to that of the local velocity vector (bold symbols), or $\mathbf{R} = -(\eta/C)\mathbf{v}$, where η is the fluid dynamic viscosity, and C is called the conductance of a pore, which is a function of its cross-sectional shape and the location of the point. In addition, if the resisting force R_s is much larger than the convective acceleration (i.e., $\mathbf{v} \cdot \nabla v_s$) then the Navier–Stokes equation reduces to the Stokes equation, and the introduction of $\mathbf{R}$ into Eq. (3) yields:

$$\rho_w \frac{\partial v_s}{\partial t} + \frac{\eta}{C} v_s = -\rho_w g \frac{\partial z}{\partial s} - \frac{\partial p}{\partial s} \tag{4}$$

Eq. (4) can be multiplied through by $C \cdot d\sigma/ds$, where σ is the local coordinate of a particular streamline such that $v_s \approx v/(d\sigma/ds)$, yielding:

$$C\rho_w \frac{\partial v}{\partial t} + \eta v = -C\left(\frac{\partial p}{\partial s} + \rho_w g \frac{\partial z}{\partial s}\right)\frac{\partial \sigma}{\partial s} \tag{5}$$

By volume averaging Eq. (5) and applying coordinate transformation back to the fixed x-, y-, and z-directions, the average governing equation in laminar flow through a porous medium is found:

$$\overline{v}_i + \overline{C}\frac{\rho_w}{\eta}\frac{\partial \overline{v}_i}{\partial t} = -\frac{K_{ij}}{n\eta}\left(\frac{\partial \overline{p}}{\partial x_j} + \rho_w g \frac{\partial z}{\partial x_j}\right) \tag{6}$$

where the bar over the variables indicates 'average' values, n is the porosity, and K_{ij} is the permeability tensor that is a function of the average conductance of the pores (projected in the global fixed x-, y-, and z-directions). The second term in the left hand side in Eq. (6) represents local accelerations that can be neglected for low Reynolds numbers usually found in porous media. The effective (or Darcy) velocity can be found multiplying Eq. (6) by the porosity n:

$$v = -\frac{K_{ij}}{\eta}\left(\frac{\partial \overline{p}}{\partial x_j} + \rho_w g \frac{\partial z}{\partial x_j}\right) \tag{7}$$

Eq. (7) is known as Darcy's law (Eq. (2)), although in this case it is derived through upscaling the incompressible Navier–Stokes equations rather than experimentally.

3.2. Finite element model

Closed-form solutions for the hydraulic conductivity of porous media are only available for idealized and simple geometries, such as cylindrical tubes of varying radii or 'fissure' models (e.g., Kozeny's equation, Kozeny–Carman's equation, Hagen–Poiseuille equation). These models involve considerable simplification of the actual geometry of granular media. Grain particles are often randomly ordered. In real soils the geometry of the pore-network is almost invariably very complex (for example, as shown in Fig. 3b). For these cases, a closed-form derivation of the hydraulic conductivity in Darcy's Law from first-principles using the Navier–Stokes equations is impossible. For this reason, we use a numerical method to solve the governing equations on actual pore-scale geometries so as to estimate the macroscale hydraulic conductivity. The form of the Navier–Stokes equation (Eq. (3)) employed for the analysis of pore-scale fluid flow is:

$$\rho_w \frac{\partial \mathbf{v}}{\partial t} + \rho_w(\mathbf{v} \cdot \nabla)\mathbf{v} + \nabla p - \eta \nabla^2 \mathbf{v} = \mathbf{F} \tag{8}$$

where ρ_w is the fluid density, $\mathbf{v}$ is the fluid velocity field, η is the dynamic fluid viscosity, p is pressure and $\mathbf{F}$ is a volume force field of various origins (for example, gravity). An additional continuity equation completes the system:

$$\nabla \cdot \mathbf{v} = 0 \tag{9}$$

For problems of small physical size, as described here, Eq. (8) may be simplified and gravitational body forces neglected. Suitable initial and boundary conditions must be provided for this system of partial differential equations to have a unique solution.

The finite element package Comsol [22] is used to solve the fluid flow problem for the pore-network domain, which is based on the actual geometry obtained from micro-CT as described in previous subsection '3D pore geometry estimations'.

Following the procedure published by Fourie and co-workers [11], the finite element mesh is generated from the segmented 3D geometries (Fig. 3) using Simpleware's ScanFE. The mesh of the pore-network comprises 308,955 tetrahedral elements (Fig. 4a). Complete saturation of the pore spaces is assumed, with water as the permeating fluid. The analysis is for room temperature 293 K and assumes a density of $\rho_w = 1000\ \mathrm{kg/m^3}$ and a dynamic viscosity of $\eta = 0.001$ Pa s. Water is simulated to flow in the vertical direction (z-direction, Fig. 4a), as it does in the actual macroscale hydraulic conductivity tests. A pressure drop of 1.0 Pa is prescribed as the boundary condition for the both the top and bottom surfaces, which ensures the Reynolds number is much lower than 2300, and thus is comfortably in the laminar regime (i.e., Darcy's law is a good approximation).

4. Results and discussion

The finite element model of the pore-scale fluid flow is solved for steady state conditions using the High Performance Computing facilities at the University of Melbourne (64 × 1.5 GHz Itanium II processors, with a total of 256 GB shared RAM). Fig. 4b shows an example of the calculated water velocity through the pore space (five vertical slices are shown). The local velocities are clearly seen to increase as water flows through narrower pore-channels (lighter gray regions in Fig. 4b). The pore velocity tends to zero in the regions where there is no connectivity of the pores (darker gray in Fig. 4b), as water will not flow through in these regions. These 'blind' pores effectively reduce the overall hydraulic conductivity. Thus, the results show that pore connectivity plays a crucial role in determining hydraulic conductivity. In addition, Fig. 4b shows that there is no water movement near the grain surfaces (darker regions), obeying to the viscous friction captured in the Stokes equations.

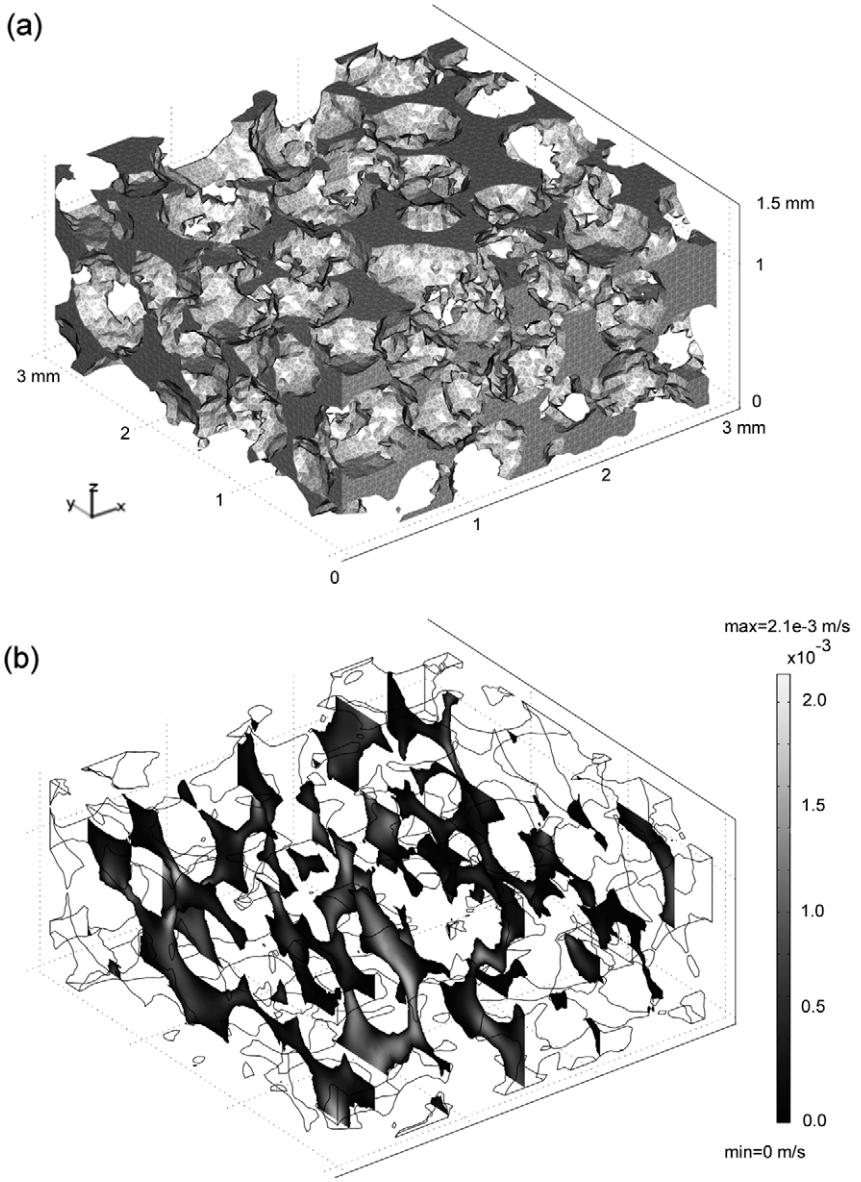

Fig. 4. Finite element model: (a) 3D mesh of the pore-network comprising 308,955 tetrahedral elements (and 1,650,714 degrees of freedom); (b) Selected slides in the vertical direction showing fluid velocity, with no movement near the grain walls (dark) and maximum velocities in narrow channels (brighter).

A complementary two-dimensional numerical analysis of the entire diametral cross-section of the specimen shows in greater detail, the preferential water flow-paths development within the pore space (Fig. 5 – geometry taken from Fig. 3). The inevitable alignment of particles against the wall of the cylindrical container results in a more ordered packing of particles adjacent to cell boundaries, which diminishes towards the centre of the specimen. This more ordered packing near the walls results in less tortuous pathways and should enhanced pore connectivity for the water flow. However, this wall effect does not seem to be particularly pronounced when looking at Fig. 5 (compare zones 1, 2 and 3). Consequently, it seems that no critical zones are discarded when selecting the 3D representative elementary volume form the bulk specimen.

The average vertical hydraulic conductivity of the 3D numerical models can be estimated from these pore-scale models by dividing the average of local pore fluid velocities $\overline{v}$ (Fig. 4b) by the average hydraulic gradient i:

$$k_{num} = \frac{\overline{v}}{i} = \frac{\frac{n}{A_{pore}} \cdot \int_{A_{pore}} v_z dA}{(\nabla p/\gamma_w)/L} \tag{10}$$

where A_{pore} is the net pore area normal to the direction of the water flow in consideration (in this case, the vertical or z-direction), n is the porosity, v_z is the local velocity within the pore space in the vertical direction, Δp is the change in pressure between the top and bottom cross-sections, and L the distance between them.

Due to computational limitations, the 3D porous media sample analysed in this work is 2.9 mm × 2.9 mm × 1.5 mm in volume (308,955 tetrahedral elements in the pore-network model); which, however, accommodates enough grain particles (from the core of the specimen) to satisfy the requirements of being a 'representative elementary volume'. Indeed, Fig. 6 shows the estimated hydraulic conductivity (k_{num}) as a function of the number of solid particles involved in the simulations for multiple realizations (black rhombi). As the number of particles increases, that is, as the control volume increases, the estimated hydraulic conductivity becomes more stable. The computational demand increases with the size of the control volume (open circles) expressed as CPU time.

The estimated hydraulic conductivity using Eq. (10) is 9.3×10^{-4} m/s. This value is seen to compare favourably in Fig. 7 with the measured macroscale hydraulic conductivity of $9.5 \pm 0.8 \times 10^{-4}$ m/s (i.e., 8.8×10^{-4} m/s to 10.4×10^{-4} m/s) obtained from the constant head permeability test on the same specimen. Therefore, the theoretical link between the macroscopic geotechnical test measurements to estimate hydraulic conductivity from Darcy's law, and the estimate based on the application of microscale fluid flow equations to micro-CT 3D geometries, is confirmed by our experimental and theoretical studies. For comparison, the prediction of hydraulic conductivity using the Kozeny–Carman equation, for uniform spheres ($C-K$ coefficient = 5) and porosity 0.35, is also shown in Fig. 7 [23].

This opens up the possibility of using state-of-the-art imaging of real 3D pore geometries and finite element analyses to predict soil properties. It is expected that further soil properties may also be estimated using this approach, including diffusion and other particulate transport processes in soils, as well as properties such as thermal and electrical conductivity.

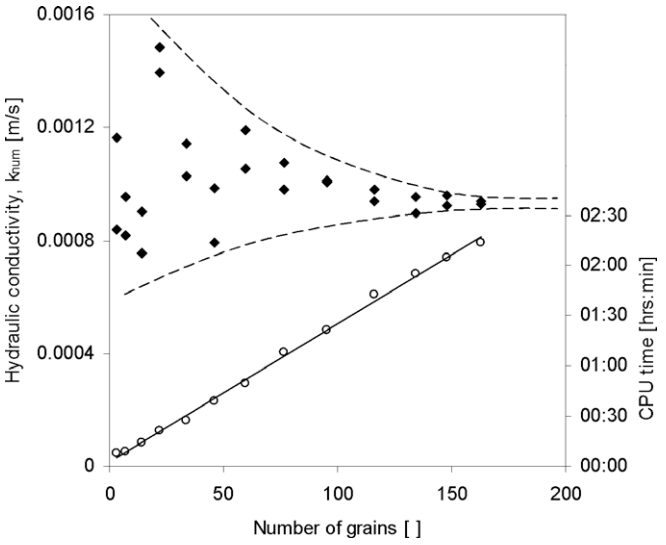

Fig. 6. Representativeness of the numerical model: variability of the estimated hydraulic conductivity with control volume size, expressed as the number of solid particles contained in it (black rhombi); and computational demand increase with the size of the control volume (open circles).

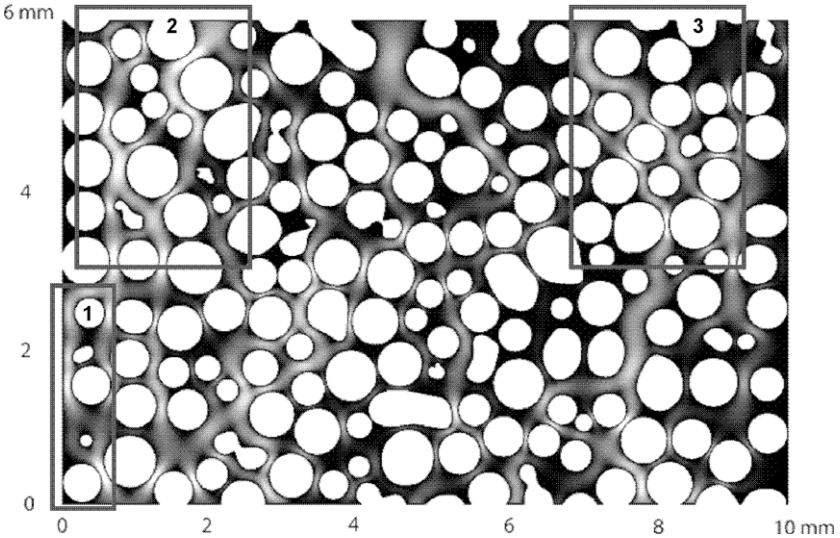

Fig. 5. Preferential flow-paths: this larger vertical cross-section of the specimen (2D) highlights the preferential water flow-paths that develop within the pore space.

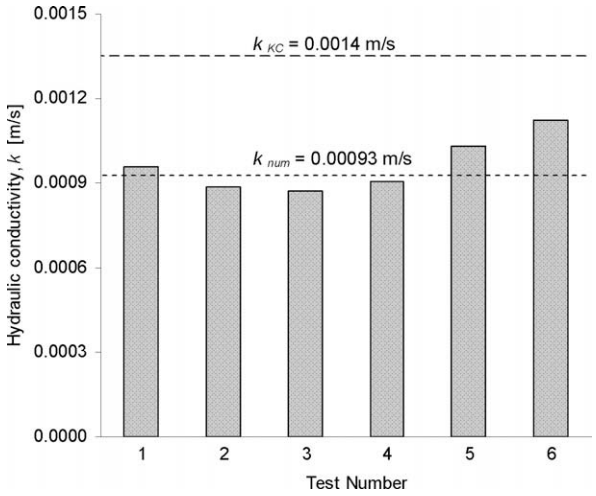

Fig. 7. Comparison between the hydraulic conductivity values obtained using Darcy's law in the physical tests (bars), the prediction by Kozeny–Carman equation (dashed line), and the estimated value from the numerical solution of the Navier–Stokes equations within the pore-network of the same specimen (dotted line).

5. Conclusions

Darcy's law is the key constitutive equation required to model ground water flow. The foundations of Darcy's law are experimental and the key parameter, the hydraulic conductivity, can be found experimentally using standardised approaches such as the constant or variable head permeameter tests. However, it is known that the hydraulic conductivity is linked to more fundamental equations describing microscale behaviour of the fluids in porous materials. This paper has summarized these theoretical links between the macroscopic phenomenological Darcy's law and the pore-scale fundamental Stokes equations, and recognised that the application of the pore-scale analysis requires characterisation of the pore-scale geometry of the porous material. State-of-the-art X-ray computer assisted micro-tomography has been employed to obtain this essential geometrical information.

This paper then posed the question: can the pore-scale geometry found using micro-CT be employed to estimate the macroscale hydraulic conductivity of a porous medium and, thus, also to verify Darcy's law? Careful experiments, using a specifically designed permeability cell were conducted to measure the hydraulic conductivity and characterise the pore-scale geometry. The results confirm that it is possible to successfully estimate the measured macroscale hydraulic conductivity for a representative volume of the porous medium by solving the Navier–Stokes equation at the pore-scale. This opens up a new approach to estimating an important soil property.

In addition, the numerical modelling allows the development of pore-scale fluid preferential flow-paths to be quantified and visualized and it highlights the importance of pore space connectivity on the transport properties of the soil. We anticipate that this approach will be used more widely, as it opens up the possibility of using state-of-the-art real 3D pore geometries and finite element analyses to estimate several other soil properties from a single micro-CT test (e.g. hydraulic, thermal and electrical conductivity).

Acknowledgements

Support for this research was provided by the Australian Research Council (ARC-DP0451576). X-ray micro-CT data were obtained by Dr. Alan Jones at the Electron Microscopy Unit (EMU), The University of Sydney. Dr. Neil Killeen and Prof. Gary Egan provided assistance with the High Performance Computing performed at The University of Melbourne, which is gratefully acknowledged.

References

[1] Mitchell JK, Soga K. Fundamentals of soil behavior. Hoboken (NJ): John Wiley & Sons; 2005.
[2] Powrie W. Contributions to geotechnique 1948–2008: groundwater. Geotechnique 2008;58(5):435–9.
[3] Sutera SP. The history of Poiseuille's law. Annu Rev Fluid Mech 1993;25:1–19.
[4] Rouse H, Ince S. History of hydraulics. Iowa City: Iowa Institute of Hydraulic Research, State University of Iowa; 1957.
[5] Brown GO. The history of the Darcy–Weisbach equation for pipe flow resistance. In: Proceedings of the environmental and water resources history; 1994. p. 34–43.
[6] Bear J. Dynamics of fluids in porous media. New York: Dover; 1988.
[7] Lambe TW, Whitman RV. Soil mechanics, SI version. New York: Wiley; 1979.
[8] Matyka M, Khalili A, Koza Z. Tortuosity–porosity relation in porous media flow. Phys Rev E (Statistic Nonlinear Soft Matter Phys) 2008;78(2):026306.
[9] Fredrich JT, DiGiovanni AA, Noble DR. Predicting macroscopic transport properties using microscopic image data. J Geophys Res 2006;111(B03201):1–14.
[10] Santamarina JC, Fam MA, Klein KA. Soils and waves. Chichester: Wiley; 2001.
[11] Fourie W, Said R, Young P, Barnes DL. The simulation of pore scale fluid flow with real world geometries obtained from X-ray computed tomography. In: Comsol conference, Newton, MA, USA; 2007. 6 p.
[12] Frost JD, Yang C-T. Effect of end platens on microstructure evolution in dilatant specimens. Soils Found 2003;43(4):1–11.
[13] Vogel HJ, Kretzschmar A. Topological characterization of pore space in soil-sample preparation and digital image-processing. Geoderma 1996;73:23–38.
[14] Aste T, Saadatfar M, Senden TJ. Geometrical structure of disordered sphere packings. Phys Rev E – Stat Nonlinear Soft Matter Phys 2005;71(6):061302.
[15] Perret J, Prasher SO, Kartzas A, Langford C. Three-dimensional quantification of macropore networks in undisturbed soil cores. Soil Sci Soc Am J 1999;63:1530–43.
[16] Wang LB, Frost JD, Lai JS. Three-dimensional digital representation of granular material microstructure from X-ray tomography imaging. J Comput Civil Eng 2004;18(1):28–35.
[17] Amin MHG, Hall LD, Chorley RJ, Carpenter TA, Richards KS, Bache BW. Magnetic resonance imaging of soil–water phenomena. Magn Reson Imag 1994;12:319–21.
[18] Deurer M, Vogeler I, Khrapitchev A, Scotter D. Imaging of water flow in porous media by magnetic resonance imaging microscopy. J Environ Qual 2002;31(2):487–93.
[19] Cnudde V, Masschaele B, Dierick M, Vlassenbroeck J, Van Hoorebeke L, Jacobs P. Recent progress in X-ray CT as a geosciences tool. Appl Geochem 2006;21(5):826–32.
[20] Santamarina JC, Fratta D. Discrete signals and inverse problems: an introduction for engineers and scientists. Hoboken (NJ): Wiley; 2005.
[21] Whitaker S. The equations of motion in porous media. Chem Eng Sci 1966;21(3):291–300.
[22] COMSOL-AB. Comsol Multiphysics User's Guide. Stockholm; 2007.
[23] Carrier WDI. Goodbye, Hazen; hello, Kozeny–Carman. J Geotech Geoenviron Eng 2003;129(11):1054–6.